Influences of phosphorus concentration and porewater advection on phosphorus dynamics in carbonate sands around the Weizhou Island, northern South China Sea

Zhiming Ning[a], Cao Fang[a], Kefu Yu[a,*], Bin Yang[b,*], Solomon Felix Dan[b], Ronglin Xia[a], Yukun Jiang[a], Ruihuan Li[c], Yinghui Wang[a]

[a] *Guangxi Laboratory on the Study of Coral Reefs in the South China Sea, Coral Reef Research Centre of China, School of Marine Sciences, Guangxi University, Nanning 530004, PR China*
[b] *Guangxi Key Laboratory of Marine Disaster in the Beibu Gulf, Beibu Gulf University, Qinzhou 535011, PR China*
[c] *State Key Laboratory of Tropical Oceanography, South China Sea Institute of Oceanology, Chinese Academy of Sciences, Guangzhou 510301, PR China*

ARTICLE INFO

ABSTRACT

A series of flow-through reactor experiments were undertaken to assess the potential effect of porewater advection and dissolved inorganic phosphorus (DIP) concentration on benthic DIP dynamics in permeable sediments collected from the Weizhou Island, northern South China Sea. The flux of DIP ranged from -0.13 to 0.05 mmol m^{-2} h^{-1}, and the reversal from DIP efflux to influx occurred when the DIP concentration reached a threshold. DIP release from the sediment into the seawater peaked at intermediate advection rate, which perhaps provide optimum conditions for DIP release related to $CaCO_3$ dissolution. Phosphorus limitation in seawater could be relieved by DIP release from the sediment, and $CaCO_3$-bound P in carbonate sands may play a major role in benthic DIP release and decrease in the molar nitrogen/phosphorus ratio in seawater around the Weizhou Island.

1. Introduction

Phosphorus (P) is an important biogenic element that limits algal growth, influences primary productivity, and biogeochemical cycling of other biogenic elements such as carbon (C) and nitrogen (N), and has been identified as the biolimiting nutrient in numerous coastal marine ecosystems around the world (Tyrrell, 1999; Xu et al., 2008; Jiang et al., 2014). Rivers are the major pathway through which land-derived organic matter with associated nutrients including P are transported to the ocean (Benitez-Nelson, 2000) although recent studies have shown that submarine ground water discharge could also play a significant role in supplying terrestrial nutrients to aquatic environments (Jeong et al., 2012; Zhang et al., 2017; Wang et al., 2020). In overall, surface sediment serves as a natural repository for organic matter and nutrients, and plays important roles in the biogeochemical cycling of P in marine environments (Paytan and McLaughlin, 2007).

Shallow water coral reefs extend over ~0.1% of the marine environment, and are mostly found in warm and/or oligotrophic waters, which span across ~30° N to 30° S, where the reefs are influenced by a lot of environmental stressors, including over-fishing, climate change, and eutrophication due to anthropogenic nutrient input (Hoegh-Guldberg et al., 2017). However, the complexity of coral reefs makes them hotspots for marine biodiversity as diverse aquatic species obtain their food and habitation from coral reef ecosystem (Reaka-Kudla, 1997). Despite the fact that coral reefs thrive in oligotrophic waters, their productivity is nevertheless high (Crossland et al., 1991), and may be linked to efficient nutrient recycling processes, in addition to the presence of organisms with characteristics photosynthetic endosymbionts (Ferrier-Pagès et al., 2016). On the other hand, diffusive fluxes of nutrients in organic-poor and coarse-grained carbonate sediments seem to have little contribution to primary productivity of coral reefs. Nevertheless, studies have shown that porewater advection can enhance the rate at which organic matter is mineralized, which makes permeable sandy sediments being active biogeochemical reactors (Rocha, 2008; Bourke et al., 2017), and thus, play important roles in the cycling of C, N, and P in coral reef ecosystems (Rasheed et al., 2002, 2004; Monbet et al., 2007).

Human activities affect not only nutrient concentration, but also nutrient ratio and structure. The classic Redfield stoichiometric ratio of N and P (N/P = 16) is generally and often used to judge whether N or P

---

is the ultimate limiting nutrient for primary productivity. Because P cannot be fixed from the atmosphere input unlike N, it is often considered as the ultimate limiting nutrient in many coastal marine ecosystems (e.g., Tyrrell, 1999; Xu et al., 2008; Jiang et al., 2014; Dan et al., 2019). The limitation of P in coral ecosystems negatively affects the resistance of corals to environmental stresses (Wiedenmann et al., 2013). Thus, P limitation in coral reef ecosystems becomes interesting for future research (Ferrier-Pagès et al., 2016).

Benthic nutrient fluxes in permeable sediments can decrease the N/P ratio of the overlying seawater (Ning et al., 2019). Thus, it is necessary to improve the understanding of P cycling in reef sediments. Benthic P flux varies in both flux direction and strength under different environmental conditions (Alongi et al., 2008; Seidel et al., 2015; Ning et al., 2016). Studies have shown that benthic P flux is higher at sites closer to coastline than at sites far away from coastline (e.g., Monbet et al., 2007), and it tends to be higher in silty than in sandy sediments (Alongi et al., 2008). These differences are somewhat related to the amount of organic matter in sediments, but in most cases the enrichment of organic matter does not seem to have positive effects on benthic P release in fine sandy sediments (Sospedra et al., 2017). Furthermore, greater P uptake occurs in carbonate sand than in silicate sand (Ning et al., 2019), as P could be bound to the surface of the carbonate grains and/or taken up by microphytobenthic communities (Rasheed et al., 2004; Monbet et al., 2007). During laboratory incubation studies involving continuous samples shanking, Suzumura et al. (2002) showed that the calcium carbonate bound P can be rapidly released into the overlying seawater as dissolved reactive P. However, the role of benthic P flux in coral reef ecosystems has only been sporadically studied (Rasheed et al., 2003; Furnas et al., 2011), and its influences by environmental factors such as porewater advection in permeable sediments are yet unclear.

Weizhou Island is located in a relatively high latitude area in the northern South China Sea, and coral reefs are distributed around the island (Fig. 1). Anthropogenic activities on the island have increased the concentrations of N, resulting in elevated N/P ratio in seawater around the island (Yu et al., 2019). Considering the ecological importance of this island with respect to coral reef, we investigated P concentration both in the seawater and in sediments, and evaluated the flux of P in permeable sediments around the island in September 2019. We compared the data in this study with those obtained in May 2018 from Ning et al. (2019) to assess the temporal variation in chemical characteristics of the seawater and sediment around the Weizhou Island and their impacts on benthic P flux. In this paper, we hypothesize that porewater advection enhances DIP release rates in permeable carbonate sediments. In order to test this hypothesis, we implemented a series of

flow-through reactor (FTR) experiments with various advection rates or P amendment to obtain further information on the interaction between benthic P dynamics and $CaCO_3$ precipitation/dissolution. A better understanding of the benthic P dynamics in permeable sediments under various conditions may help address the broader issue of P cycling in coral reef ecosystem.

2. Materials and methods

2.1. Study sites and sampling

Weizhou Island, located in the Beibu Gulf, northern of South China Sea, is ~48 km off the southern China mainland coast (Fig. 1). Because the Weizhou Island is situated in a relatively high subtropical latitude, it provides an ideal habitat for coral growth. The corals are mainly distributed in water depths less than 10 m (Yu et al., 2019). The island has been developed as a tourism site, and the south bay of the Weizhou Island has been widely used for scallop culture for decades. On the island, there are no large rivers flowing to the sea. The main reason for the rapid coral reef degeneration is escalating anthropogenic impact, such as seawater pollution, unsustainable tourism and aquaculture activities (Yu et al., 2019).

At stations with the water depth of ~0.5 m (Fig. 1), seawater samples were collected by submersing a 10 l acid-cleaned polyethylene bottle, and sediments (0–10 cm) were collected by pushing Plexiglas tubes (inner diameter of 10 cm) into the sediment. Within 2 h of collection, sediment and unfiltered seawater samples were taken back to the laboratory for FTR experiment. In the field, the temperature and salinity of seawater were measured using a YSI ProDSS multiparameter probe. The probe sensor was calibrated using a combination of known standard calibration solution and fresh water (see ProDSS user manual). A Rhizon soil moisture sampler (19.21.23F Rhizon CSS) was pushed into the sediment in the field, and the sampler was connected to a 10 ml vacuum tube to extract porewater at depths of 0–5 cm. The seawater and porewater samples for nutrient analysis were filtered with 0.45 μm pore-size syringe filters, and were frozen at − 20 °C until later analysis. In addition, the sediment samples for chemical analysis were placed in ziploc plastic bags, and then frozen at − 20 °C prior to analysis. Samples were analyzed within one month after collection.

2.2. Flow through reactor (FTR) experiments

The FTR experiment was implemented according to Ning et al. (2019) using Plexiglas columns (inner diameter of 4 cm and height of 10 cm) and lids designed by Rao et al. (2007), in which radial grooves
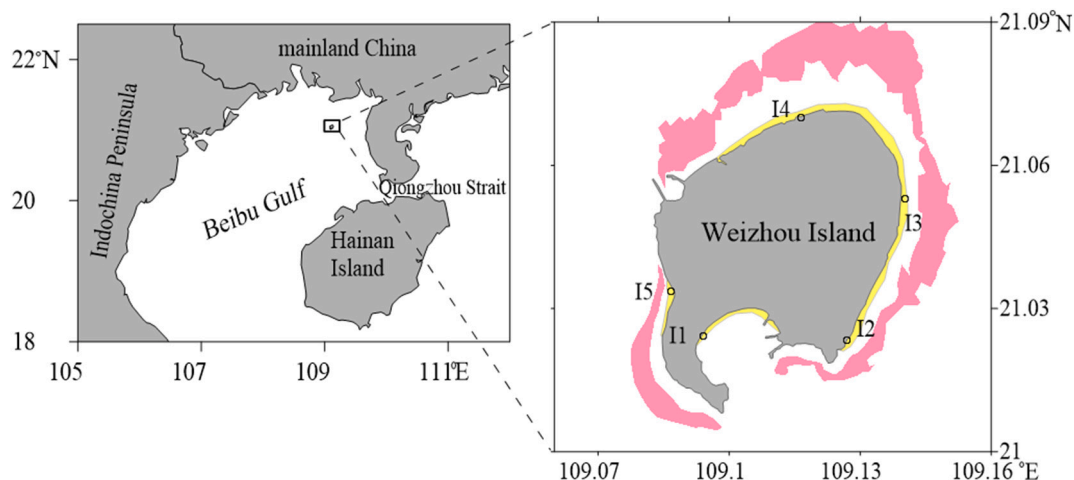

Fig. 1. Sampling stations in the tidal flats (the yellow areas) around the Weizhou Island. The red areas are coral covering areas. (For interpretation of the references to color in this figure legend, the reader is referred to the web version of this article.)

were milled around the inflow and outflow ports. Briefly, homogenized sediment was packed into each Plexiglas column. Seawater was pumped from the bottom up through the sediments at variable flow rates (see below) from a large carboy, with continuous air flushing. The sides of the sediment columns were covered with aluminium foil to allow light penetration only to the top of the columns. During incubations, the sediment columns were immersed in an outdoor tank filled with seawater (28–30 °C). Flux measurements began 6 h after the start of the core percolation to acclimatize under the laboratory condition. The measurements of both inflow and outflow characteristics were conducted twice, with the intervals of 1 h, and the duration of flux measurement was within 2 h. At each sampling time, seawater samples for nutrient analysis, including Ca^{2+} and Fe^{2+} were collected directly from the outflow, and the inflow seawater samples were collected from the source using 60 ml syringes. 40 ml of each seawater sample was filtered through 0.45 μm pore-size syringe filters and frozen at -20 °C. Additionally, the dissolved oxygen (DO), and the pH of inflow and outflow seawater were measured using a multiparameter probe (YSI ProDSS), and the precision was < 5% coefficient of variation (CV). The FTR experiments were carried out in duplicate.

Three FTR experiments were performed in this study. In the first experiment, sediments and seawater collected from each station were incubated to investigate the benthic DIP dynamics. In the second experiment, all the sediments collected from different stations were mixed and repacked in FTRs, and different DIP doses were added into the inflow seawater with the final DIP concentrations of 0.15, 0.23, 0.35, 2.50 and 3.15 μmol l^{-1}, respectively. The influent DIP concentrations were within the concentration range previously reported in the Weizhou Island seawater and sediment porewater (Ning et al., 2019). The porewater flow rate in the former two experiments was maintained at 1 ml min^{-1} (equivalent to 48 l m^{-2} h^{-1}), with a residence time of 1 h, but the rate in the natural environment are highly variable both spatially and temporally. Thus, it is important to assess how porewater advection could control benthic fluxes. In the third experiment, mixed sediments were used as in the second experiment, and the seawater without P amendment was pumped through the FTRs at variable flow rates (1, 2 and 3 ml min^{-1}, respectively). These rates (equivalent to 48, 96 and 144 l m^{-2} h^{-1}, respectively) are typical in coral reefs (Santos et al., 2012).

2.3. Analytical methods and calculations

Nutrient concentrations were measured using an autoanalyzer (QuAAtro, SEAL Analytical). The precisions for NH_4^+, NO_2^-, NO_3^-, and dissolved inorganic phosphorus (DIP) analyses were < 6% CV (Ning et al., 2019). Concentrations of the dissolved inorganic nitrogen (DIN) were obtained as the sum of NO_3^-, NO_2^- and NH_4^+. Alkalinity was determined by Gran titration (precision < 0.2%). The pH and alkalinity in the inflow and outflow seawater of each FTR were used to calculate the dissolved inorganic carbon (DIC) and aragonite saturation state (Ω_{Ar}) using the Excel macro CO2SYS (Lewis et al., 1998). Dissolved Fe (assumed to be present as Fe^{2+}) was measured by inductively coupled plasma optimal emission spectroscopy, while Ca^{2+} was measured by ethylene glycol tetraacetic acid titrations (Tsunogai et al., 1968). The precisions were < 5% CV.

Each frozen sediment sample was freeze-dried, and then the $CaCO_3$ content was measured through acid-base titration according to Müller, 1966. The total organic carbon (TOC) content was determined using a CHNOS Elemental Analyser (Vario EL III, Elemental Analyser). Prior to the determination, inorganic carbon was removed via acidification with 4 mol l^{-1} HCl (Ning et al., 2016). The inorganic P (IP) content in sediments was determined using a procedure involving extraction with 1 mol l^{-1} HCl, and analyzed for DIP. To determine total P (TP), the sediment samples were combusted at 550 °C for 2 h, extracted with HCl, and analyzed as IP. The concentration of organic P (OP) content was estimated by subtracting IP from TP contents (Aspila et al., 1976; Yang

et al., 2018). All samples were analyzed in triplicates, with measurement precision less than 5% CV.

Fluxes (mmol m^{-2} h^{-1}) were calculated from the differences in the concentrations of DIP, DIN, DO, DIC, Ca^{2+} and Fe^{2+} between the influent and effluent seawater, flow rate, and cross-sectional area of the sediment column according to Eq. (1) (Santos et al., 2012; Ning et al., 2019). In parallel, the yield/uptake of DIP from/by sediment (μmol g^{-1} wet sediment) was calculated from the difference in DIP concentration between the influent and effluent seawater, volume of seawater in FTR, and the weight of wet sediments according to Eq. (2), since DIP yield/uptake should also be related to the amounts of sediment in addition to flow rate. Positive values represent efflux out of the sediment, while negative values represent influx into the sediment.

$$F = (C_{out} - C_{in}) \times R/S \tag{1}$$

$$F = (C_{out} - C_{in}) \times V/m \tag{2}$$

where C_{in} and C_{out} are the concentrations of DIP, DIN, DO, DIC, Ca^{2+} and Fe^{2+} in the influent and effluent seawater, respectively. R is the flow rate, S is the cross-sectional area of the sediment column (12.56 cm^2), V is the volume of seawater in FTR (48–58 ml), and m is the weight of wet sediments (220–230 g wet weight).

The data was subjected to a one-way analysis of variance (ANOVA) to know whether the variations and distributions of the measured parameters were statistically significant at the 95% confidence level. Pearson's correlation analysis with a two-tailed test of significance was carried out to evaluate the relationship between the measured parameters. All statistical analyses were performed using a Statistical Package for the Social Sciences (SPSS) software (version 22.0), and the statistical significance was judged at the criterion of $p < 0.05$.

3. Results

3.1. Chemical characteristics of the surface seawater and sediment around the Weizhou Island

There was no significant difference in the physical and chemical characteristics of the surface seawater at different stations around the Weizhou Island (ANOVA; $p > 0.05$; $n = 10$) (Table 1). However, seawater temperature and salinity in September 2019 were slightly lower than those in May 2018. The concentration of DIN in September was approximately twice the level measured in May, while the concentration of DIP was lower in September than in May. Thus, the DIN/DIP ratio in September 2019 ranged from 26.6 to 350, while the DIN/DIP ratio in May 2018 was 11.5–21.7, closer to the Redfield N/P ratio of 16:1.

The concentrations of DIN and DIP in sediment porewater samples were higher than those in the overlying seawater (Table 1). Porewater DIN concentration in September 2019 was higher than that in May 2018, but the opposite abundance was found for DIP, such that the DIN/DIP ratio became significantly higher in September 2019 than in May 2018. Concentration of Fe^{2+} in porewater was as low as 1.05 μmol l^{-1}, and the highest concentration was found at station I5 in September 2019. $CaCO_3$ contents in the sediments at stations I3, I4 and I5 (representing carbonate sediment) were approximately twice the level at stations I1 and I2 (representing silicate sediment). Low levels of organic content were observed in the Weizhou Island sands, and the highest concentrations of TOC and OP were recorded at station I2. The molar TOC/OP ratio in all the investigated stations was higher than the Redfield C/P ratio of 106:1. IP was the dominant sedimentary P form in the Weizhou Island sediments, and OP constituted only a smaller part (6.1–28%) of the sedimentary TP pool (Table 1). Concentrations of sedimentary IP correlated significantly with the $CaCO_3$ content in carbonate sediments (Fig. 2).

Table 1
Physical and chemical characteristics of the surface seawater and sediment around the Weizhou Island during May 2018 and Sep. 2019. The data of May are from Ning et al. (2019). The acronyms T, S, DIN, DIP, and TOC represents temperature, salinity, dissolved inorganic nitrogen, dissolved inorganic phosphorus, and total organic carbon, respectively.

| Time	Station	Seawater					Sediment								
		T (°C)	S (psu)	DIN (μmol l⁻¹)	DIP (μmol l⁻¹)	DIN/DIP	DIN (μmol l⁻¹)	DIP (μmol l⁻¹)	DIN/DIP	Fe²⁺ (μmol l⁻¹)	CaCO₃ (%)	TOC (%)	IP (μmol g⁻¹)	OP (μmol g⁻¹)	TOC/OP
May	I1	32.5	32.40	3.26	0.27	11.9	6.52	0.68	9	1.28	40	0.04	0.20	0.05	667
	I2	28.7	32.35	4.74	0.24	19.9	349	1.78	196	4.12	34	0.12	0.34	0.11	909
	I3	33.3	32.10	2.31	0.16	14.9	11.9	1.12	11	1.35	67	0.07	0.26	0.08	748
	I4	30.5	32.30	3.16	0.28	11.5	9.81	2.79	4	1.05	72	0.06	0.45	0.09	556
	I5	31.7	32.38	5.69	0.26	21.7	7.14	2.04	4	1.31	61	0.04	0.23	0.09	379
	Means	**31.3**	**32.31**	**3.84**	**0.24**	**16.0**	**76.9**	**1.68**	**45**	**1.57**	**55**	**0.07**	**0.30**	**0.08**	**652**
Sep.	I1	30.5	30.59	5.39	0.02	350	16.6	0.46	36	1.48	42	0.04	0.32	0.04	891
	I2	29.4	30.26	11.09	0.08	144	225	0.54	418	1.15	26	0.04	0.36	0.09	380
	I3	29.7	31.51	2.88	0.08	37.5	114	0.54	213	1.43	70	0.04	0.52	0.03	995
	I4	29.4	30.04	6.63	0.15	43.1	67.5	0.50	135	1.36	69	0.02	0.30	0.08	172
	I5	30.0	30.24	11.47	0.43	26.6	158	0.69	229	7.74	64	0.03	0.31	0.07	361
	Means	**29.8**	**30.53**	**7.49**	**0.15**	**120**	**104**	**0.57**	**206**	**2.80**	**54**	**0.03**	**0.36**	**0.06**	**560**
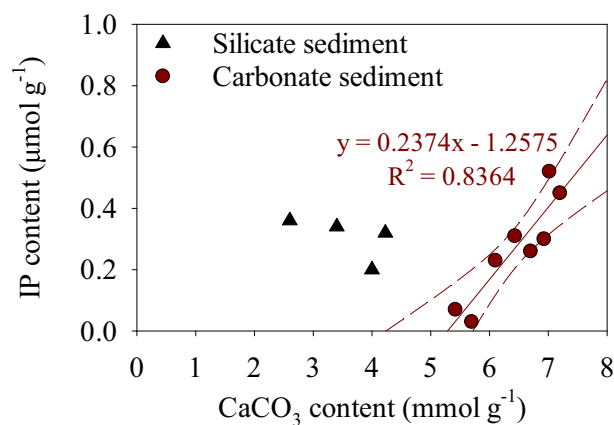
Fig. 2. Linear relationship between IP and CaCO₃ contents in carbonate sediments around the Weizhou Island. Dashed lines represent 95% confidence intervals.
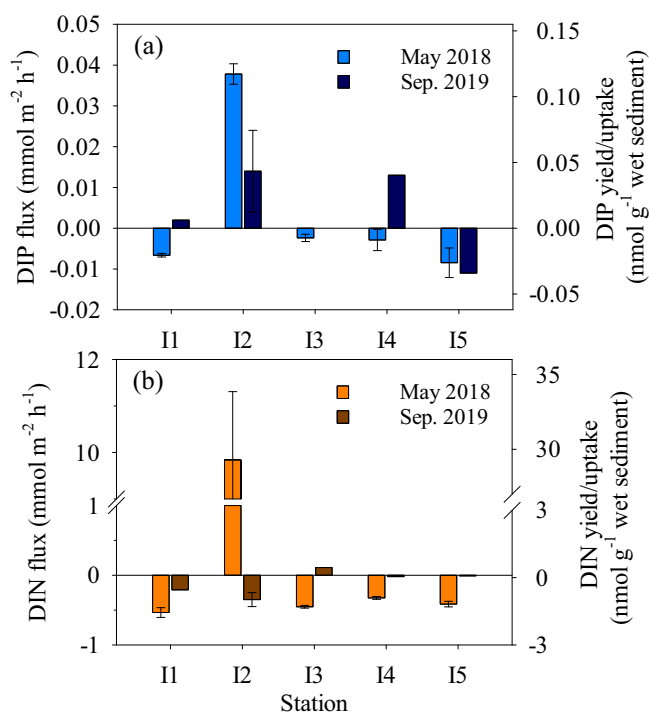
$$y = 0.2374x - 1.2575$$
$$R^2 = 0.8364$$

Fig. 3. Benthic fluxes (or expressed as the yield/uptake) of (a) DIP and (b) DIN at the investigated sites in the Weizhou Island during May 2018 and Sep. 2019. The May data are from Ning et al. (2019). The error bars show SD.

3.2. The first FTR experiment: benthic P flux at different stations

In the first experiment, the DIP flux varied at different stations and differed in the two periods (Fig. 3a). At most of the stations, DIP was transferred from the seawater to the sediment in May with the exception of station I2, and released from the sediment into the seawater in September with the exception of station 15 (Fig. 3a). DIP flux correlated with OP content in sediments, but had no correlations with the fluxes of DO, DIC, Ca²⁺ and Fe²⁺, but the relationship between the fluxes of DO, DIC, and Ca²⁺ was significant (Table 2). The fluxes of DO, DIC, Ca²⁺ and Fe²⁺ at different stations during the two investigated period are shown in Table S1. DIN was transferred from seawater to the sediment at most of the investigated stations (Fig. 3b). In September, considerable DIN influx was only observed at stations I1 and I2 with the highest DIN/DIP ratio in seawater. Flowing through the sediments, the DIN/DIP ratio in the effluent seawater decreased in comparison with those in the

Table 2

Correlation analysis results for OP in sediments and fluxes of DO, DIC, Ca^{2+}, DIN, DIP and Fe^{2+} obtained from the first FTR experiment.

	OP	DO flux	DIC flux	Ca^{2+} flux	DIN flux	DIP flux	Fe^{2+} flux
OP	1	−0.63*	0.14	0.26	0.36*	0.42*	0.11
DO flux	−0.63*	1	−0.41*	−0.36*	−0.46*	−0.31	−0.24
DIC flux	0.14	−0.41*	1	0.41*	0.39*	0.21	0.29
Ca^{2+} flux	0.26	−0.36*	0.41*	1	0.07	−0.16	−0.04
DIN flux	0.36*	−0.46*	0.39*	0.07	1	0.64*	0.27
DIP flux	0.42*	−0.31	0.21	−0.16	0.64*	1	−0.01
Fe^{2+} flux	0.11	−0.24	0.29	−0.04	0.27	−0.01	1

* Correlation is significant at the 0.05 level. $n = 40$.
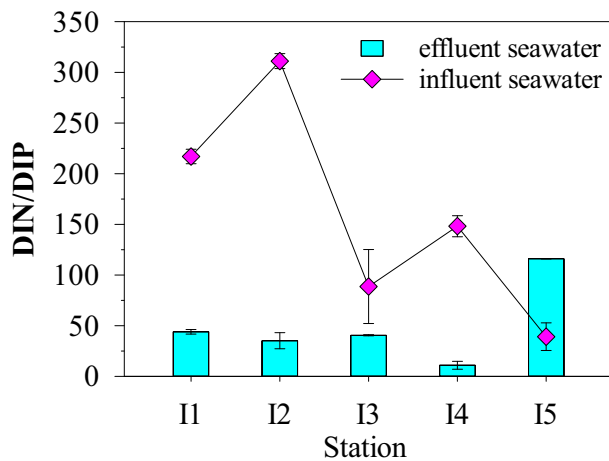
Fig. 4. The molar ratio of DIN to DIP in the inflow and the outflow streams through sediments at the Weizhou Island.

influent seawater; the exception was at station I5 where DIP uptake resulted in an increase of DIN/DIP ratio in seawater (Fig. 4).

3.3. The second FTR experiment: benthic P flux under the changing DIP concentration in seawater

In the second experiment, DIP was released from the sediment into the seawater in the incubation groups with the concentrations of 0.15, 0.23 and 0.35 µmol l^{-1}, respectively, and was transferred from the seawater to the sediment with the concentrations of 2.50 and 3.15 µmol l^{-1}, respectively (Fig. 5a). The fluxes of DIP significantly correlated with DIP concentration in the inflow seawater, and the reversal from DIP efflux to influx occurred when the concentration of DIP reaches the threshold of 0.40 ± 0.06 µmol l^{-1}. Similarly, the fluxes of Ca^{2+} significantly correlated with DIP concentration in the inflow seawater, and Ca^{2+} was transferred from the seawater to the sediment when the DIP concentration was higher than 1.11 ± 0.35 µmol l^{-1} (Fig. 5b). However, the data obtained from the first experiment deviated from the regression line of DIP concentration and DIP flux (Fig. 5).

3.4. The third FTR experiment: benthic P flux under variable advection rates

The consumption rate of DO (i.e., DO influx) increased with increasing advection rate, and then plateaued at advection rates higher than 96 l m^{-2} h^{-1} (Fig. 6a), but the flux of DIP was highest at the intermediate advection rate (Fig. 6b). The Ca^{2+} flux also peaked at the intermediate advection rate (Fig. 6c). The sediments exposed to advection rates as high as 144 l m^{-2} h^{-1} should experience high DIP flux calculated from DO fluxes, however, the DIP flux was the lowest (Fig. 6b). Correspondingly, the Fe^{2+} flux was highest at the advection rate of 144 l m^{-2} h^{-1} (Fig. 6d).
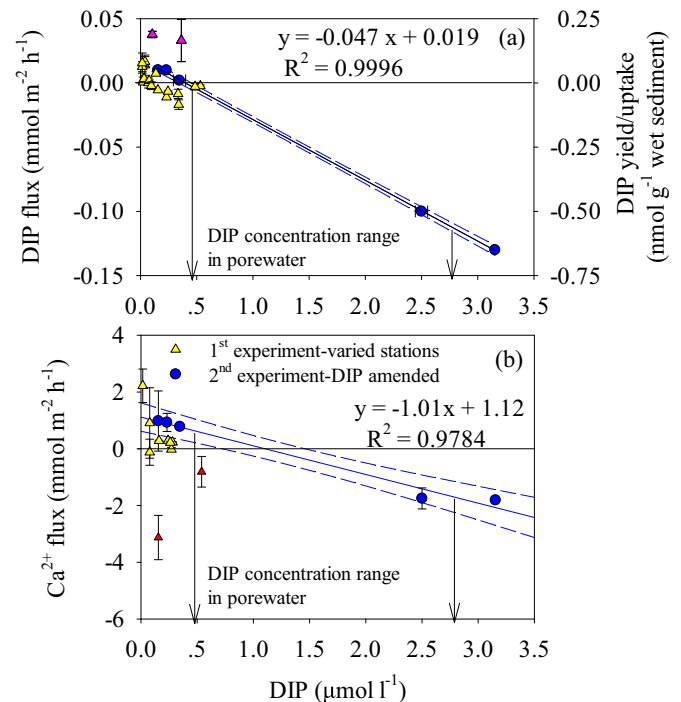
Fig. 5. Relationship between benthic (a) DIP flux (or expressed as the yield/uptake), (b) Ca^{2+} flux and DIP concentrations in the influent seawater. The triangles and circles represent the results obtained from the first and second experiments, respectively. Especially, the pink triangles represent the results at station I2 in May 2018, and the red triangles represent the results at stations I4 and I5 in September 2019. The grey areas represent the in situ DIP concentration range in porewater. (For interpretation of the references to color in this figure legend, the reader is referred to the web version of this article.)

4. Discussion

4.1. Benthic P dynamics around the Weizhou Island and its effects on nutrient structure in seawater

Based on the average DIN/DIP ratio (Table 1), P limitation occurred in the aquatic environment around the Weizhou Island in September 2019, but the range of DIN/DIP ratio in the same area was within the normal nutrient (i.e., N/P) regime in May 2018. Although such temporal variation may be seasonal, increasing anthropogenic activities could also play a role in nutrient variability. Previous study had found that nutrient structure varies seasonally in seawater around the Weizhou Island with changes in the DIN/DIP ratio from 25 in winter to 135 in summer due to increase in freshwater input from mainland China in summer (Han et al., 2015). Recent studies have also reported that the concentrations of DIN together with the molar DIN/DIP ratios around the Weizhou Island have been increasing annually, due to increase in anthropogenic activities including sewage discharge, unsustainable tourism activities, and aquaculture practices (Han et al.,
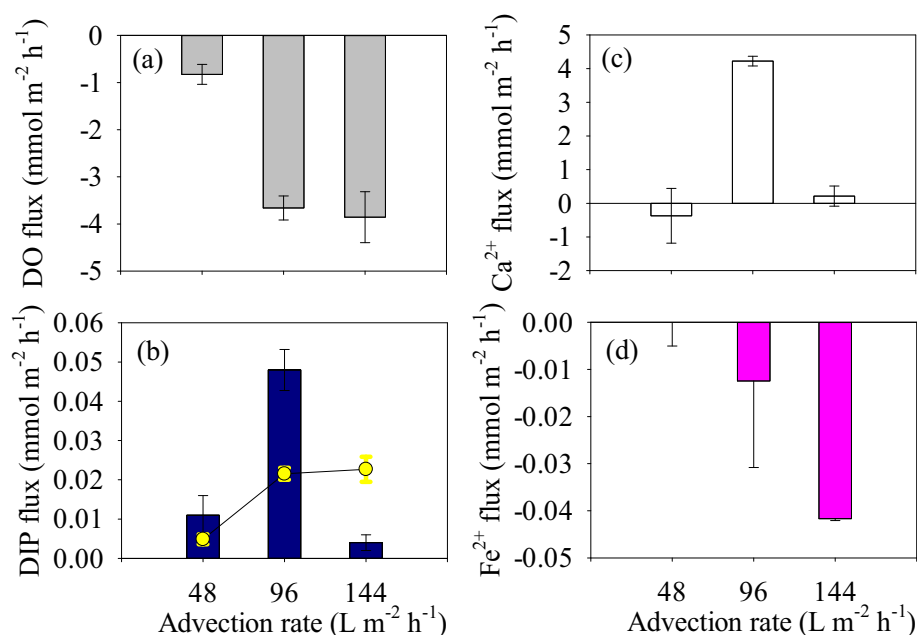
Fig. 6. Fluxes of (a) DO, (b) DIP, (c) Ca^{2+} and (d) Fe^{2+} under different advection conditions. The error bars show the SD. The yellow points in panel b are DIP fluxes calculated from DO fluxes based on the $-DO/DIP$ ratio of 170 ± 10. (For interpretation of the references to color in this figure legend, the reader is referred to the web version of this article.)

2015; Yu et al., 2019). As observed in this study, P limitation in seawater could be relieved by nutrient exchanges between sediments and seawater, but the extent at which the exchanges occur varied at different stations (Fig. 4). Firstly, the uptake of DIN by sediments is important for the reduction of DIN/DIP ratio in seawater. The DIN transferred into sediments from seawater can participate in microalgal uptake, microbial N cycling, and adsorption in sediments (Erler et al., 2014). The N_2 flux at the same sites of the Weizhou Island investigated in September 2019 was 0.04–0.34 mmol m^{-2} h^{-1} (Z. Ning et al., unpublished data), which corresponds to the level of DIN influx (Fig. 3b). Thus, N-loss by denitrification in permeable sediments plays an important role in reduction of DIN/DIP ratio in seawater. Alternatively, DIP release from sediments could directly relieve P limitation in seawater. Benthic P flux varies both in flux direction and strength at different sites during the investigated two periods (Fig. 3a), because DIP flux depends on a lot of factors, such as OP remineralization, occurrences of $CaCO_3$ precipitation/dissolution, reductive dissolution of Fe oxides, and oxidative precipitation of Fe^{2+} (Monbet et al., 2007; Ferrier-Pagès et al., 2016).

The remineralization of OP results in DIP release from sediments, and DIP flux was tightly coupled to OP content in sediments (Table 2). The highest DIP efflux was found at station I2, which recorded the highest OP content in sediment, probably because of terrestrial input with abundant organic matters at this site. Previous study had reported that the spatial variation of TOC around the Weizhou Island was due to varying terrestrial input (Ning et al., 2019). Generally, the high TOC/OP ratio in sediments around the Weizhou Island indicates the influence of terrigenous organic matter, because terrigenous organic matter is mostly characterized by elevated molar TOC/OP ratios, ranging from 300 to 1300 (Ruttenberg and Goñi, 1997; van der Zee et al., 2002). The DO flux provides a proxy for the integrated benthic mineralization rate, but the oxidations of reduced inorganic components (e.g., NH_4^+, Fe^{2+}, or sulfide) are important sinks of DO. As described and validated in previous study (Ning et al., 2019), the outflows of FTRs were still oxic, suggesting that aerobic mineralization dominated the organic matter oxidation, and the reduction of other terminal electron acceptors (e.g., oxidized iron, or sulfate) may have had little contribution. This is also consistent with the previous finding that iron and sulfate reduction remain insignificant in reef sands (Werner et al., 2006). Indeed, the Fe^{2+} concentration in porewater was low and the Fe^{2+} flux was negligible when compared with the DO flux (Table S1). Thus, DO flux could

be explained as the mineralization of organic matter, and the DIP release from OP remineralization could be calculated based on DO flux and -O_2/C/N/P ratio of $170 \pm 10/117 \pm 14/16 \pm 1/1$ (Anderson and Sarmiento, 1994). The higher concentration of DIP in porewater and greater influx of DO in May 2018 than those in September 2019 indicated that more active OP remineralization occurred in May 2018 than in September 2019. However, DIP was transferred to sediment from the seawater at most of the stations (Fig. 3a), and there was no significant relationship between DO flux and DIP flux (Table 2), which indicates that there may be other processes related to the IP in sediments that influences the benthic DIP flux.

Sedimentary TP pool was dominated by IP in the Weizhou Island sediments (Table 1). Sedimentary IP has been sequentially separated into four fractions, which include the exchangeable or loosely adsorbed P, ferric (Fe)-bound P, authigenic apatite P (Ca-P), and detrital apatite P in coral reef sediments (Monbet et al., 2007). Among the different sedimentary IP fractions, Ca-P has been reported to be dominant in carbonate sediments (Monbet et al., 2007; Joy et al., 2019). Significant correlation between sedimentary IP and $CaCO_3$ in this study (Fig. 2), indicates that in the Weizhou Island sediments, Ca-P is the dominant IP fraction. Thus, the occurrence of $CaCO_3$ precipitation/dissolution is supposed to be an important factor influencing DIP flux in the studied coral reef sediments. In other words, DIP should be released from Ca-P during $CaCO_3$ dissolution or combines with $CaCO_3$ during $CaCO_3$ precipitation. However, Ca^{2+} flux as an indicator of the $CaCO_3$ precipitation/dissolution rate did not significantly relate to DIP flux at different stations during the two studied periods (Table 2). This result may be due to the complex effects from diverse factors such as the DIP concentration in seawater (Suzumura et al., 2002), sediment permeability, mineral composition (Ning et al., 2019) and organic matter content (Rasheed et al., 2003) on DIP flux at different studied stations. Although $CaCO_3$ precipitation occurred in carbonate sediments in September 2019 (Table S1), the DIP flux at different stations exhibited opposite direction (Fig. 3a). The dissimilarity in the direction of DIP flux may have resulted from higher DIP concentration at station I5 compared to station I4 (Table 1). This is because the enrichment of DIP in seawater generally results in considerable uptake of DIP by sediments (Suzumura et al., 2002). To rule out the dissimilarity in characteristics of seawater and sediments at different stations, the second FTR experiment using the mixed sediments and seawater was conducted to obtain further information on the role of Ca-P in benthic DIP flux under

the changing DIP concentrations as discussed in Section 4.2 below.

4.2. Impacts of DIP concentration in seawater on P dynamics in permeable sediments

The concentration of DIP in seawater varied by a factor of 10 around the Weizhou Island, and the benthic DIP flux was tightly related to the concentration of DIP in seawater after ruling out the dissimilarity in sediments at different stations in the second FTR experiment. The transfer of DIP to the sediments may be favourable for $CaCO_3$ calcification and Ca-P formation, as $CaCO_3$ calcification occurred under condition of the high DIP concentration (Fig. 5b). This observation is consistent with the previous finding that carbonate sediments efficiently trap P through strong adsorption of DIP onto $CaCO_3$ particles (Monbet et al., 2007). The mechanism involves initial adsorption of DIP at the surface kink sites of $CaCO_3$ particles, followed by incorporation of some surface-associated DIP into the crystal structure as growth occurs (Walter and Burton, 1986; House and Donaldson, 1986).

The dissolution of $CaCO_3$ occurred when DIP concentration was lower than 1.11 ± 0.35 μmol l^{-1}, as the inhibition of $CaCO_3$ dissolution by adsorption of DIP at surface kink sites was weakened (Walter and Burton, 1986). However, there was no DIP release from the sediment to the seawater when DIP concentration was in the range of 0.40–1.11 μmol l^{-1}, indicating that the released DIP from $CaCO_3$ dissolution was still adsorbed by the $CaCO_3$ particles under the intermediate concentration of DIP in seawater. Only when the DIP concentration was lower than 0.40 ± 0.06 μmol l^{-1}, both adsorbed and co-precipitated P were released with the dissolution of $CaCO_3$, which happened to relieve P limitation in seawater. The tightly coupled relationship between DIP in seawater and $CaCO_3$ precipitation/dissolution in sediments also explains why the concentrations of sedimentary IP exhibited a linear relationship with $CaCO_3$ content in carbonate sediments (Fig. 2). In fact, the data obtained from the first FTR experiment deviated from the regression line of DIP concentration and DIP flux (Fig. 5). The first reason is that the dominant DIP release pathway from the sediment may be remineralization of OP rather than $CaCO_3$ dissolution at sites with higher OP content (such as station I2). The second reason may be due to the dissimilarity in seawater characteristics such as pH and Ω_{Ar}. Great Ca^{2+} influx was observed at stations I4 and I5 with the high Ω_{Ar} in seawater (Table S1), due to negative correlation between Ca^{2+} flux of carbonate sediments and the Ω_{Ar} of the overlying seawater (Eyre et al., 2018; Ning et al., 2019), even with the fact that DIP concentration was lower than 1.11 ± 0.35 μmol l^{-1} (Fig. 5b). The Ω_{Ar} was > 1 at the outlet of all the FTRs (data are not shown), but $CaCO_3$ dissolution still occurred at $\Omega_{Ar} > 1$, which suggests that the bulk porewater Ω_{Ar} may not be the actual condition at the site of dissolution. This could be due to the presence of microzones of high pCO_2 caused by aerobic respiration in intragranular pores of $CaCO_3$ grain, and the diagenesis-dependent low pH in microzones may have facilitated dissolution (Kessler et al., 2020). Porewater advection also transports DO into the permeable sediment, which stimulates aerobic respiration and enhances dissolution (Cyronak et al., 2014).

4.3. Impacts of porewater advection rates on P dynamics in permeable sediments

Previous studies have assessed the limitations in the use of FTR, which represents a 1-dimensional, steady state, and unidirectional system, and the fluxes obtained from the FTR should be seen as potential in situ rates (Santos et al., 2012; Ning et al., 2019). Comparisons between fluxes obtained from the FTR experiments with other approaches need to be undertaken with care, because the direction of flow, advective rates, and the length of sediment column are different. In fact, porewater advection rates in the natural environment are highly variable spatially and temporally (Santos et al., 2012). In this study, the variation of DO consumption rate was consistent with the findings

reported for other study areas (Rasheed et al., 2004; Cook et al., 2007; Glud et al., 2008; Santos et al., 2012). The DIP release rates from organic matter remineralization calculated from DO fluxes increased with advection rates (Fig. 6b). However, a major discrepancy between the total and remineralization-dependent fluxes of DIP suggests that a large portion of DIP release was derived from sedimentary IP pool. This is consistent with previous study of Suzumura et al. (2002) who reported that desorption of P from $CaCO_3$ particles represents an important pathway, which supplies DIP from carbonate sediment to the overlying seawater. The highest DIP flux was observed at the intermediate advection rate, but little is known about the mechanism. This could be explained based on a tentative conceptual model from Santos et al. (2012), and according to the four premises in this study. First, the pool of Ca-P in sediments significantly affects DIP flux. Second, the $CaCO_3$ precipitation/dissolution is controlled by Ω_{Ar} in seawater. Third, diagenesis-dependent $\Omega_{Ar} < 1$ in microzones of the $CaCO_3$ grain pores are sites for dissolution, although bulk porewater Ω_{Ar} was > 1. Fourth, higher DIP concentration inhibits $CaCO_3$ dissolution.

At low advection rate ($48 \, l \, m^{-2} \, h^{-1}$), porewater probably follows a tortuous path around the grains (Santos et al., 2012). There is longer time for DO consumption and DIP release from OP remineralization in sediment column. However, DIP adsorption on the surface of sediment grains due to low advection rate may inhibit the dissolution of $CaCO_3$. At high advection rate ($144 \, l \, m^{-2} \, h^{-1}$), DO concentration around and within the sand grains is expected to increase (Santos et al., 2012), preventing the development of $\Omega_{Ar} < 1$ microenvironments within the grains. Meanwhile, higher DO concentrations within the grains allow for the formation of Fe oxides that bind P (van Helmond et al., 2020). At intermediate advection rate ($96 \, l \, m^{-2} \, h^{-1}$), seawater within grains would be partially flushed creating a steep oxygen gradient in porous sands (Santos et al., 2012). Since the Ω_{Ar} in the inner parts of the grains may be < 1, the DO transferred from the outer parts into the inner parts would facilitate organic matter mineralization, and the diagenesis-dependent low pH would also facilitate dissolution, which is accompanied by DIP release. The release of DIP could be brought from the inner parts to the outer parts by intermediate advection, rather than being adsorbed by the $CaCO_3$ particles under low advection rates. Thus, intermediate advection would be suitable for $CaCO_3$ dissolution and substantial release of DIP. This rate is typically found on continental shelves, implying that the $CaCO_3$ precipitation/dissolution in carbonate sands may play a major role in P cycling in coral reefs.

4.4. Comparison of P content in sediments of the Weizhou Island and worldwide coastal areas

Bulk sedimentary P pool contributes to the DIP levels in the overlying seawater and plays important roles in P cycling in coral reefs (Suzumura et al., 2002; Ferrier-Pagès et al., 2016). The concentrations of P in surface sediments around the Weizhou Island were lower than the levels reported for other study areas as shown in Table 3. The differences are related in part to the texture of sediment, as fine-grained sediments dominated by clay and/or silt have stronger affinity with organic matter and P than coarse sandy sediments (Dan et al., 2020a). Thus, the content of P is expected to be lower in coral reefs permeable sediments as observed in this study. On the other hand, terrestrial and anthropogenic influence may account for higher P content in reef sediments as reported for the Kavaratti island, Indian Ocean (Joy et al., 2019) and Great Barrier Reef (Alongi et al., 2006; Monbet et al., 2007). However, the input of terrigenous organic matter with elevated TOC/OP ratio may also contribute to low OP content (especially if the OP is relatively labile) in sediments. According to the official data published by local government (http://xxgk.beihai.gov.cn/bhshjbhj/tszl_84510/hbxxgk/swrfz/index.html), the TOC/OP ratio of suspended particulate matter in sewage outlet water of a wastewater treatment plant on the Weizhou Island is ~167, and the ratio in untreated wastewater could be twice that of treated wastewater. In addition, the OP produced by

Table 3

Comparison of the IP and OP contents in the surface sediments of the Weizhou Island with other worldwide coastal areas, including reef areas. Values in parentheses indicate the percentage of the OP form with regard of total phosphorus.

Locations	IP content (μmol g^{-1})	OP content (μmol g^{-1})	References
Maowei Sea, northern Beibu Gulf	2.9–16	1.1–12 (25–56%)	Yang et al., 2019
northern South China Sea	4.6–15	0.47–5.8 (7.2–32%)	Yang et al., 2018
Cross River estuary, West Africa	7.1–16	0.32–2.9 (13%)	Dan et al., 2020b
Mid and outer shelf of Great Barrier Reef	6.0–11	2.4–3.7 (16–28%)	Monbet et al., 2007
Arlington and Sudbury Reefs, Great Barrier Reef	11–14[a]		Alongi et al., 2006
reefs of Ishigaki Island, Japan	6.1–7.2	0.92–1.1 (13%)	Suzumura et al., 2002
reefs of the Florida Keys, USA	< 0.19[a]		Szmant and Forrester, 1996
reefs of Kavaratti island, Indian Ocean	0.61 ± 0.16	4.2 ± 1.5 (87%)	Joy et al., 2019
Weizhou Island, northern South China Sea	0.20–0.52	0.03–0.11 (6.1–28%)	This study

[a] The value represented total phosphorus content in sediments.

organisms in the water column could be readily remineralized before reaching the sediment or at the early stage of diagenesis in the uppermost sediments, resulting in low OP concentration and large fraction of refractory OP component in reef sediments (Suzumura et al., 2002). All these may help explain why OP constituted only a smaller fraction of the sedimentary TP pool in different study areas (Table 3). At least, most of the anthropogenic and natural P input in the coastal waters from land appears to be taken up by the nearshore algae before reaching patch reef areas (Szmant and Forrester, 1996), and this accounted for the lower content of P in reef sediments of the Florida Keys as shown in Table 3. In summary, the relatively low P content in sediments around the Weizhou Island is somewhat related to sediment textures, terrestrial supply of organic matter with higher TOC/OP ratios and biogeochemical processes.

5. Conclusions

This study evaluated the benthic phosphorus (P) dynamics in permeable sediments under the changing environments around the Weizhou Island, surrounded by coral reefs. The higher DIN/DIP in seawater and the high TOC/OP ratio in sediments pointed to P limitation in the aquatic environment around the Weizhou Island. The release of DIP from sediments and uptake of DIN in sediments could help address the lingering higher DIN/DIP ratio in seawater around the Weizhou Island. The potential fluxes of DIP at different stations were positively related to OP content in sediments, but the relatively low OP content in sediments around the Weizhou Island makes it difficult for benthic DIP efflux to make up for the deficiency of P in the water column. However, intermediate advection rate enhanced sedimentary CaCO$_3$ dissolution and accompanied DIP release, implying that CaCO$_3$-bound P in carbonate sands may play a major role in P cycling in coral reefs. Furthermore, the reversal from DIP efflux to influx occurred when the concentration of DIP in seawater reaches a threshold of 0.40 ± 0.06 μmol l^{-1}, which could be coupled to adsorption and coprecipitation of P on CaCO$_3$ particles in sediments.

CRediT authorship contribution statement

Zhiming Ning: Conceptualization, Methodology, Investigation, Writing. **Cao Fang:** Methodology, Investigation, Data curation. **Kefu Yu:** Resources, Supervision, Project administration. **Bin Yang:** Conceptualization, Formal analysis, Supervision. **Solomon Felix Dan:** Writing - Review & Editing. **Ronglin Xia:** Investigation, Resources. **Yukun Jiang:** Investigation, Validation. **Ruihuan Li:** Validation, Visualization. **Yinghui Wang:** Project administration.

Declaration of competing interest

The authors declare that they have no known competing financial interests or personal relationships that could have appeared to influence the work reported in this paper.

Appendix A. Supplementary data

Supplementary data to this article can be found online at https://doi.org/10.1016/j.marpolbul.2020.111668.

References

Alongi, D.M., Pfitzner, J., Trott, L.A., 2006. Deposition and cycling of carbon and nitrogen in carbonate mud of the lagoons of Arlington and Sudbury Reefs, Great Barrier Reef. Coral Reefs 25 (1), 123–143.

Alongi, D.M., Trott, L.A., Pfitzner, J., 2008. Biogeochemistry of inter-reef sediments on the northern and central Great Barrier Reef. Coral Reefs 27 (2), 407–420.

Anderson, L.A., Sarmiento, J.L., 1994. Redfield ratios of remineralization determined by nutrient data analysis. Glob. Biogeochem. Cycles 8 (1), 65–80.

Aspila, K.I., Agemian, H., Chau, A.S.Y., 1976. A semi-automated method for the determination of inorganic, organic and total phosphate in sediments. Analyst 101 (1200), 187–197.

Benitez-Nelson, C.R., 2000. The biogeochemical cycling of phosphorus in marine systems. Earth Sci. Rev. 51, 109–135.

Bourke, M.F., Marriott, P.J., Glud, R.N., Hasler-Sheetal, H., Kamalanathan, M., Beardall, J., ... Cook, P.L., 2017. Metabolism in anoxic permeable sediments is dominated by eukaryotic dark fermentation. Nature Geoscience 10 (1), 30.

Cook, P.L.M., Wenzhöfer, F., Glud, R.N., Janssen, F., Huettel, M., 2007. Benthic solute exchange and carbon mineralization in two shallow subtidal sandy sediments: effect of advective porewater exchange. Limnol. Oceanogr. 52 (5), 1943–1963.

Crossland, C.J., Hatcher, B.G., Smith, S.V., 1991. Role of coral reefs in global ocean production. Coral Reefs 10, 55–64.

Cyronak, T., Schulz, K.G., Santos, I.R., Eyre, B.D., 2014. Enhanced acidification of global coral reefs driven by regional biogeochemical feedbacks. Geophys. Res. Lett. 41 (15), 5538–5546.

Dan, S.F., Liu, S.M., Udoh, E.C., Ding, S., 2019. Nutrient biogeochemistry in the Cross River estuary system and adjacent Gulf of Guinea, South East Nigeria (West Africa). Cont. Shelf Res. 179, 1–17.

Dan, S.F., Lan, W., Yang, B., Han, L., Xu, C., Lu, D., Kang, Z., Huang, H., Ning, Z., 2020a. Bulk sedimentary phosphorus in relation to organic carbon, sediment textural properties and hydrodynamics in the northern Beibu Gulf, South China Sea. Mar. Pollut. Bull. 155, 111176.

Dan, S.F., Liu, S., Yang, B., 2020b. Geochemical fractionation, potential bioavailability and ecological risk of phosphorus in surface sediments of the Cross River estuary system and adjacent shelf, South East Nigeria (West Africa). J. Mar. Syst. 201, 103244.

Erler, D.V., Santos, I.R., Eyre, B.D., 2014. Inorganic nitrogen transformations within permeable carbonate sands. Cont. Shelf Res. 77, 69–80.

Eyre, B.D., Cyronak, T., Drupp, P., De Carlo, E.H., Sachs, J.P., Andersson, A.J., 2018.

Coral reefs will transition to net dissolving before end of century. Science 359 (6378), 908–911.

Ferrier-Pagès, C., Godinot, C., D'angelo, C., Wiedenmann, J., Grover, R., 2016. Phosphorus metabolism of reef organisms with algal symbionts. Ecol. Monogr. 86 (3), 262–277.

Furnas, M., Alongi, D., McKinnon, D., Trott, L., Skuza, M., 2011. Regional-scale nitrogen and phosphorus budgets for the northern (14°S) and central (17°S) Great Barrier Reef shelf ecosystem. Cont. Shelf Res. 31 (19–20), 1967–1990.

Glud, R.N., Eyre, B.D., Patten, N.L., 2008. Biogeochemical responses to mass coral spawning at the Great Barrier Reef: effects on respiration and primary production. Limnol. Oceanogr. 53 (3), 1014–1024.

Han, L.J., Zheng, X.Q., Lan, W.L., Shi, X.F., Li, T.S., 2015. Variations of nutrients concentration in surface seawater in adjacent area of Weizhou Island in recent 10 years. J. Appl. Oceanogr. 34 (1), 65–72 (in Chinese with English abstract).

Hoegh-Guldberg, O., Poloczanska, E., Skirving, W., Dove, S., 2017. Coral reef ecosystems under climate change and ocean acidification. Front. Mar. Sci. 4 (158), 1–20.

House, W.A., Donaldson, L., 1986. Adsorption and coprecipitation of phosphate on calcite. J. Colloid Interface Sci. 112 (2), 309–324.

Jeong, J., Kim, G., Han, S., 2012. Influence of trace element fluxes from submarine groundwater discharge (SGD) on their inventories in coastal waters off volcanic island, Jeju, Korea. Appl. Geochem. 27, 37–43.

Jiang, Z., Liu, J., Chen, J., Chen, Q., Yan, X., Xuan, J., Zeng, J., 2014. Responses of summer phytoplankton community to drastic environmental changes in the Changjiang (Yangtze River) estuary during the past 50 years. Water Res. 54, 1–11.

Joy, A., Anoop, P.P., Rajesh, R., Mathew, A., Gopinath, A., 2019. Spatial variability of biochemical composition in coral reef sediments of Kavaratti and Pitti islands, Lakshadweep archipelago. Indian J. Geo Mar. Sci. 48 (03), 369–378.

Kessler, A.J., Rogers, A., Cyronak, T., et al., 2020. Pore water conditions driving calcium carbonate dissolution in reef sands. Geochim. Cosmochim. Acta 279, 16–28.

Lewis, E., Wallace, D., Allison, L.J., 1998. Program Developed for CO2System Calculations, Carbon Dioxide Information Analysis Center. Oak Ridge National Laboratory, Oak Ridge, Tenn.

Monbet, P., Brunskill, G.J., Zagorskis, I., Pfitzner, J., 2007. Phosphorus speciation in the sediment and mass balance for the central region of the Great Barrier Reef continental shelf (Australia). Geochim. Cosmochim. Acta 71 (11), 2762–2779.

Müller, G., 1966. Grain size, carbonate content, and carbonate mineralogy of recent sediments of the Indian Ocean off the eastern coast of Somalia. Naturwissenschaften 53 (21), 547–550.

Ning, Z., Liu, S., Zhang, G., Ning, X., Li, R., Jiang, Z., … Zhang, J., 2016. Impacts of an integrated multi-trophic aquaculture system on benthic nutrient fluxes: a case study in Sanggou Bay, China. Aquac. Environ. Interact. 8, 221–232.

Ning, Z., Yu, K., Wang, Y., Huang, X., Han, M., Zhang, J., 2019. Carbon and nutrient dynamics of permeable carbonate and silicate sands adjacent to coral reefs around Weizhou Island in the northern South China Sea. Estuar. Coast. Shelf Sci. 225, 106229.

Paytan, A., McLaughlin, K., 2007. The oceanic phosphorus cycle. Chem. Rev. 107, 563–576.

Rao, A.M., McCarthy, M.J., Gardner, W.S., Jahnke, R.A., 2007. Respiration and denitrification in permeable continental shelf deposits on the South Atlantic Bight: rates of carbon and nitrogen cycling from sediment column experiments. Cont. Shelf Res. 27 (13), 1801–1819.

Rasheed, M., Badran, M.I., Richter, C., Huettel, M., 2002. Effect of reef framework and bottom sediment on nutrient enrichment in a coral reef of the Gulf of Aqaba, Red Sea. Mar. Ecol. Prog. Ser. 239, 277–285.

Rasheed, M., Badran, M.I., Huettel, M., 2003. Influence of sediment permeability and mineral composition on organic matter degradation in three sediments from the Gulf of Aqaba, Red Sea. Estuar. Coast. Shelf Sci. 57 (1–2), 369–384.

Rasheed, M., Wild, C., Franke, U., Huettel, M., 2004. Benthic photosynthesis and oxygen consumption in permeable carbonate sediments at Heron Island, Great Barrier Reef, Australia. Estuar. Coast. Shelf Sci. 59 (1), 139–150.

Reaka-Kudla, M., 1997. Global biodiversity of coral reefs: a comparison with rainforests. In: Reaka-Kudla, Wilson, W.P. (Eds.), Biodiversity II: Understanding and Protecting Our Biological Resources. Joseph Henry Press, Washington, USA, pp. 83–108.

Rocha, C., 2008. Sandy sediments as active biogeochemical reactors: compound cycling in the fast lane. Aquat. Microb. Ecol. 53 (1), 119–127.

Ruttenberg, K.C., Goñi, M.A., 1997. Phosphorus distribution, C:N:P ratios, and $\delta^{13}C_{oc}$ in arctic, temperate, and tropical coastal sediments: tools for characterizing bulk sedimentary organic matter. Mar. Geol. 139, 123–145.

Santos, I.R., Eyre, B.D., Glud, R.N., 2012. Influence of porewater advection on denitrification in carbonate sands: evidence from repacked sediment column experiments. Geochim. Cosmochim. Acta 96, 247–258.

Seidel, M., Beck, M., Greskowiak, J., Riedel, T., Waska, H., Suryaputra, I.N., … Dittmar, T., 2015. Benthic-pelagic coupling of nutrients and dissolved organic matter composition in an intertidal sandy beach. Marine Chemistry 176, 150–163.

Sospedra, J., Falco, S., Morata, T., Rodilla, M., 2017. Influence of organic enrichment and *Spisula subtruncata* (da Costa, 1778) on oxygen and nutrient fluxes in fine sand sediments. Estuar. Coasts 40 (3), 726–740.

Suzumura, M., Miyajima, T., Hata, H., Umezawa, Y., Kayanne, H., Koike, I., 2002. Cycling of phosphorus maintains the production of microphytobenthic communities in carbonate sediments of a coral reef. Limnol. Oceanogr. 47 (3), 771–781.

Szmant, A.M., Forrester, A., 1996. Water column and sediment nitrogen and phosphorus distribution patterns in the Florida Keys, USA. Coral Reefs 15 (1), 21–41.

Tsunogai, S., Nishimura, M., Nakaya, S., 1968. Complexometric titration of calcium in the presence of larger amounts of magnesium. Talanta 15 (4), 385–390.

Tyrrell, T., 1999. The relative influences of nitrogen and phosphorus on oceanic primary production. Nature 400 (6744), 525–531.

van der Zee, C., Slomp, C.P., Van Raaphorst, W., 2002. Authigenic P formation and reactive P burial in sediments of the Nazaré canyon on the Iberian margin (NE Atlantic). Mar. Geol. 185, 379–392.

van Helmond, N.A.G.M., Robertson, E.K., Conley, D.J., Hermans, M., Slomp, C.P., 2020. Removal of phosphorus and nitrogen in sediments of the eutrophic Stockholm archipelago, Baltic Sea. Biogeosciences 17 (10), 2745–2766.

Walter, L.M., Burton, E.A., 1986. The effect of orthophosphate on carbonate mineral dissolution rates in seawater. Chem. Geol. 56 (3–4), 313–323.

Wang, Q., Li, H., Zhang, Y., Wang, X., Xiao, K., Zhang, X., Dan, S.F., 2020. Submarine groundwater discharge and its implication for nutrient budgets in the western Bohai Bay, China. J. Environ. Radioact. 212, 106132.

Werner, U., Bird, P., Wild, C., Ferdelman, T., Polerecky, L., Eickert, G., Jonstone, R., Hoegh-Guldberg, O., de Beer, D., 2006. Spatial patterns of aerobic and anaerobic mineralization rates and oxygen penetration dynamics in coral reef sediments. Mar. Ecol. Prog. Ser. 309, 93–105.

Wiedenmann, J., D'Angelo, C., Smith, E.G., Hunt, A.N., Legiret, F.E., Postle, A.D., Achterberg, E.P., 2013. Nutrient enrichment can increase the susceptibility of reef corals to bleaching. Nat. Clim. Chang. 3 (2), 160.

Xu, J., Yin, K., He, L., Yuan, X., Ho, A.Y.T., Harrison, P.J., 2008. Phosphorus limitation in the northern South China Sea during late summer: influence of the Pearl River. Deep-Sea Res. I Oceanogr. Res. Pap. 55 (10), 1330–1342.

Yang, B., Liu, S.M., Zhang, G.L., 2018. Geochemical characteristics of phosphorus in surface sediments from the continental shelf region of the northern South China Sea. Mar. Chem. 198, 44–55.

Yang, B., Zhou, J.B., Lu, D.L., Dan, S.F., Zhang, D., Lan, W.L., … Cui, D.Y., 2019. Phosphorus chemical speciation and seasonal variations in surface sediments of the Maowei Sea, northern Beibu Gulf. Marine Pollution Bulletin 141, 61–69.

Yu, W., Wang, W., Yu, K., Wang, Y., Huang, X., Huang, R., … Chen, X., 2019. Rapid decline of a relatively high latitude coral assemblage at Weizhou Island, northern South China Sea. Biodiversity and Conservation 28 (14), 3925–3949.

Zhang, Y., Li, H., Xiao, K., Wang, X., Lu, X., Zhang, M., An, A., Qu, W., Wan, L., Wang, X., Jiang, X., 2017. Improving estimation of submarine groundwater discharge using radium and radon tracers: application in Jiaozhou Bay, China. J. Geophys. Res. Oceans 122, 1–15.